

# Using frequency response function and wave propagation for locating damage in plates

Ser-Tong Quek\* and Puat-Siong Tua<sup>‡</sup>

Department of Civil Engineering, National University of Singapore, 1 Engineering Drive 2,  
Singapore 117576

(Received August 16, 2005, Accepted November 2, 2007)

**Abstract.** In this study, the frequency domain method which utilizes the evaluation of changes in the structural mode shape is adopted to identify regions which contain localized damages. Frequency response function (FRF) values corresponding to the modal frequency, analogous to the mode shape coefficients, are used since change in natural frequency of the system is usually insignificant for localized damage. This method requires only few sensors to obtain the dynamic response of the structure at specific locations to determine the FRF via fast-Fourier transform (FFT). Numerical examples of an aluminum plate, which includes damages of varying severity, locations and combinations of multiple locations, are presented to demonstrate the feasibility of the method. An experimental verification of the method is also done using an aluminum plate with two different degrees of damage, namely a half-through notch and a through notch. The inconsistency in attaining the FRF values for practical applications due to varying impact load may be overcome via statistical averaging, although large variations in the loading in terms of the contact duration should still be avoided. Nonetheless, this method needs special attention when the damages induce notable changes in the modal frequency, such as when the damages are of high severity or cover more extensive area or near the boundary where the support condition is modified. This is largely due to the significant decrease in the frequency term compared to the increase in the vibration amplitude. For practical reasons such as the use of limited number of sensors and to facilitate automation, extending the resolution of this method of identification may not be efficient. Hence, methods based on wave propagation can be employed as a complement on the isolated region to provide an accurate localization as well as to trace the geometry of the damage.

**Keywords:** identify damage regions; mode shape; frequency response function (FRF); fast-Fourier transform (FFT).

---

## 1. Introduction

In the works by Quek, *et al.* (2003a, 2004) and Tua, *et al.* (2004a, b) for the NDE of plates and pipes based on the time-of-flight analysis of propagating waves, the robustness of the time-history method has been discussed and verified experimentally. In some applications, this method may not be the most efficient when extremely large structures are being assessed for cracks. This is due to the dispersive nature of waves and its high amplitude attenuation over long traveling distance that complicates the signal analysis leading to high degree of uncertainty in the results.

To provide a more efficient method for the entire NDE procedure, a method to reduce the region of

---

\*Professor, Corresponding Author, E-mail: [cveqst@nus.edu.sg](mailto:cveqst@nus.edu.sg)

<sup>‡</sup>Research student, E-mail: [g0202138@nus.edu.sg](mailto:g0202138@nus.edu.sg)

the structure for propagating wave assessment is necessary. To regionalize the damage location from a global to a regional (or sometimes elemental) scale, many frequency domain methods have been considered. Common ones include monitoring of changes in natural frequency (Cawley and Adams 1979, Salawu 1997), stiffness (Sampaio, *et al.* 1999) or flexibility (Pandey and Biswas 1994, although each has its own shortcomings. For example, although the decrease in the frequency may be indicative of the declining structural health state, it is unable to provide information on the region or location of damage as it only gives a global assessment (Pandey and Biswa 1994). Moreover, to cause a change in the natural frequency will require a significant defect particularly for large structures (Kim, *et al.* 2003) and hence may be unsuitable for small or localized defects such as cracks. Likewise, the monitoring of localized changes within the stiffness matrices requires higher modal frequencies to produce a significant change, which can only be effected through excitation of higher modes as well as using more sensors. Such requirements becomes more difficult with increasing order of the mode.

Another frequency domain method for detecting damage is the use of frequency response function (FRF). By performing a curve-fitting on the resultant FRF spectrum, structural parameters such as stiffness, damping and mass matrices can be computed (Ewins 1984) which are adopted as signatures for detection of damage. Some researchers (Thyagarajan 1998) advocated the direct monitoring of the FRF spectrum values. Samman and Biswas (1994a, 1994b) adopted the FRF as signatures on the structural integrity of a bridge and Sampaio, *et al.* (1999) and Owolabi, *et al.* (2003) have shown FRF to be numerically feasible for the detection and localization of damage. There exist inaccuracies in the practical computation of the FRF (Hwang 1998, Hwang and Kim 2004).

In this study, the frequency domain method which utilizes the evaluation of changes in the structural mode shape is adopted to identify damage regions for cases where change in frequency is insignificant. This method requires only few sensors to capture the response dynamics of the structure at selected locations, from which the frequency response function (FRF) are determined using Fourier spectral analysis. The method will first be illustrated, followed by numerical verifications using an analytical model of a simply-supported plate with different damage cases. The limitations of the method are also discussed. To exhibit the practical applicability of the method, an experimental verification involving a simply-supported plate will be presented.

## 2. Zoning of damage

The dynamic characteristics of a structure are influenced by its integrity. The presence of damage changes the eigen-parameters, such as natural frequencies, damping values and mode shapes, of the structure. Of these, the change in mode shapes has shown to be more appealing for structural health monitoring due to its high sensitivity to local damages compared to that relying on the change in natural frequencies.

### 2.1. Structural integrity and mode shape

Based on D'Alembert's principle, the equation of motion for a system with  $n$ -degrees of freedom may be written as follows

$$M\ddot{u} + C\dot{u} + Ku = P \quad (1)$$

where  $K$  is the stiffness matrix,  $C$  the damping matrix,  $M$  the inertia matrix of the structure,  $P$  the

applied force vector, and  $\mathbf{u}$  the displacement vector. Considering the vibration response of the undamped lumped mass system, the solution of  $\mathbf{u}$  can be expressed in the form

$$\mathbf{u} = \mathbf{U}e^{i(\omega t + \theta)} \tag{2}$$

where  $\mathbf{U}$  is an arbitrary amplitude vector. Eq. (1) then reduces to an eigenvalue problem which may be represented by

$$(\mathbf{K} - \omega_i^2 \mathbf{M}) \mathbf{u}_i = \mathbf{P}, \quad i = 1, 2, \dots, n \tag{3}$$

and  $\mathbf{u}_i$  is the  $i$ th vector amplitude of motion of the structure. From Eq. (3), it is obvious that a change in the stiffness of the structure will result in a different set of eigenvalue-eigenvector solution for the  $i$ th mode, giving a different mode shape characterized by  $\mathbf{u}_i$ .

The presence of a crack or a localized damage in a structure reduces the stiffness of the structure. Its eigen solution to Eq. (3) will be different from that of the case when the structure is in its healthy or intact state. For the case of localized damage (such as fine cracks), the change in modal frequency is insignificant and the change in eigen solution is often manifested through a change in the mode shapes.

If two sets of dynamic measurements, one for the intact or a previous known state and another for the damaged structure are taken at  $n$  different positions (or “degrees of freedom”) of the structure, the mode shapes of the two structural states can be estimated based on the frequency response function (FRF) computed from the measurements, as will be illustrated in the following sub-section. Consider the  $i$ th mode shape for the healthy (denoted as  $\mathbf{u}_i^H$ ) and damaged ( $\mathbf{u}_i^D$ ) states of the structure defined as follows

$$\mathbf{u}_i^H = [u_{i1}^H \ u_{i2}^H \ \dots \ u_{in}^H]^T \tag{4a}$$

$$\mathbf{u}_i^D = [u_{i1}^D \ u_{i2}^D \ \dots \ u_{in}^D]^T \tag{4b}$$

The relative change in mode shape coefficients,  $\Delta_i = [\delta_{i1} \ \delta_{i2} \ \dots \ \delta_{in}]^T$  for the  $i$ th mode can be obtained as

$$\delta_{ij} = \frac{(u_{ij}^D - u_{ij}^H)}{u_{ij}^H}, \quad j = 1, 2, \dots, n. \tag{5}$$

This relative change in the mode shape coefficients gives an indication of the severity in integrity difference of the current structure from the previous known state over the  $n$  monitored positions (or degrees of freedom). Each of these  $n$  positions gives a representation of the health state to a region with resolution or boundaries defined by the distance between measured positions. The highest positive difference (or relative change) of the assessed state from the previously known (or healthy) state of the structure at any of the  $n$  positions will provide an indication of possible damage occurring at the measured position. Hence, this provides a means for zoning a structure or element and identifying damaged zones, thereby reducing the required amount of “scanning” on the structure using wave propagation technique for health assessment.

The main advantage of this method is that it does not require the monitoring of many points and hence relaxes the requirement on the amount of sensors. Refined zoning onto the location of the damage can be carried out progressively by partitioning the monitoring regions into finer ones and is only constrained by practicality.

Although there are  $n$  possible mode shape that can be assessed due to the  $n$  degrees of freedom being monitored, only the relative change in first mode coefficients (i.e. for  $i = 1$  for Eqs. (4) to (5)) will be considered in this study. This is because, albeit that the higher modes are more sensitivity to localized damages, they are difficult to excite and some positions correspond to the nodal points which will exhibit small or zero relative changes. On the contrary, the first mode being the most fundamental mode can be easily excited for most structural configurations and the problem of nodal points is non-existent. This is adequate if the objective is to identify damaged zones.

2.2. Mode shape coefficients via dynamic response

The key to the method is the obtaining of reasonably accurate mode shape coefficients for computation of Eq. (5) to obtain the largest relative change for isolation of any anomalies, if present. In this study, it is proposed that the mode shape coefficients of the structure at any point may be obtained from the vibration response of the point via the computation of the FRF. An FRF is a measure of how much displacement, velocity, or acceleration response a structure has at an output DOF, per unit of excitation force at an input DOF (Schwarz and Richardson 1999), giving the receptance, mobility and inertance / acceleration FRF respectively.

To illustrate, we consider a simply supported beam as shown in Fig. 1. The theoretical mode shape for the free vibration of the beam at the seven positions indicated in Fig. 1 may be computed from Eq. (3). The first three theoretical normalized mode shapes are as shown in Fig. 2.

To obtain the mode shape coefficients for the different positions as shown Fig. 1 from the vibration response, an impact load with an excitation range covering the modal frequency band of interest (for example, Fig. 3) is induced at a non-nodal position on the beam for the required modes. The vibration response of the beam at positions where the mode shape values are required is then collected and processed using FFT to obtain their power spectrum ( $R(\omega)$ ). The reason for the choice of FFT over other signal processing techniques (such as WT, HHT, etc) is its ability to separate closely spaced

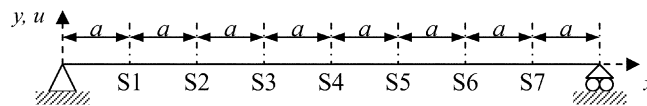


Fig. 1 Simply-supported beam with 7 monitored points equally spaced at  $a$  apart

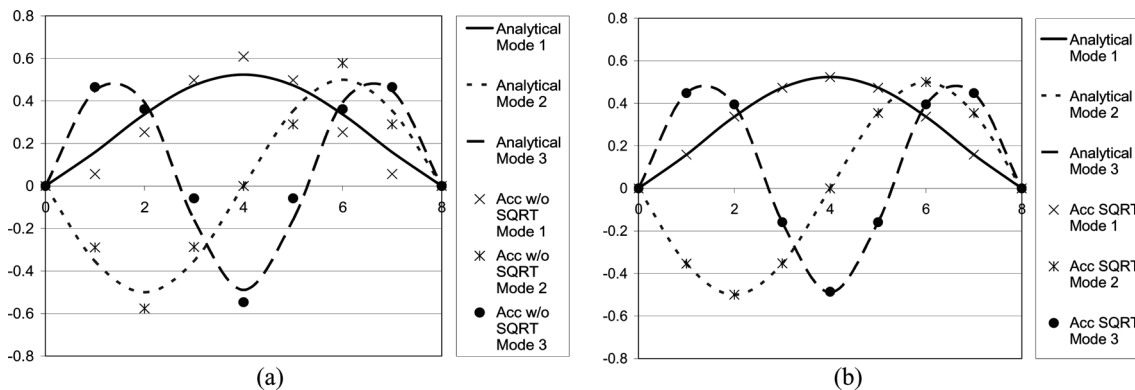


Fig. 2 Comparison of (a) power spectrum values and (b) square-rooted power spectrum values with theoretical mode shape for modes 1-3

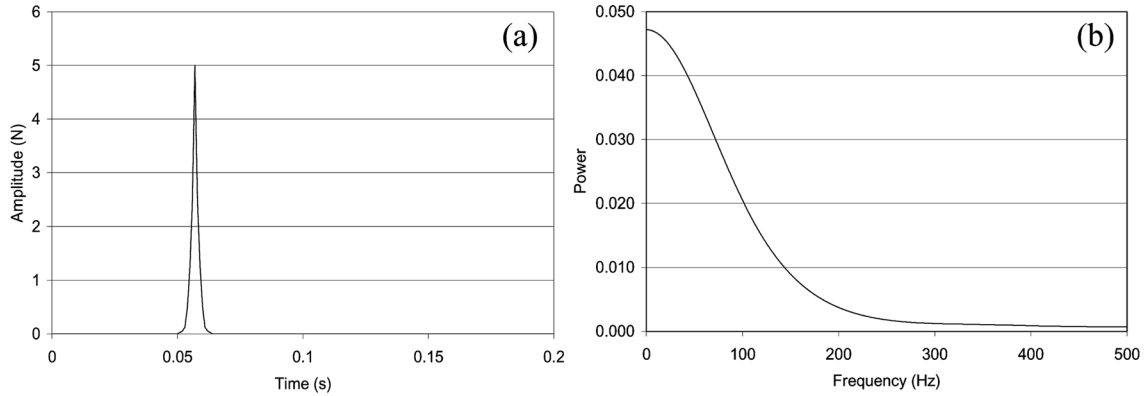


Fig. 3 (a) Impact load and corresponding (b) power spectrum

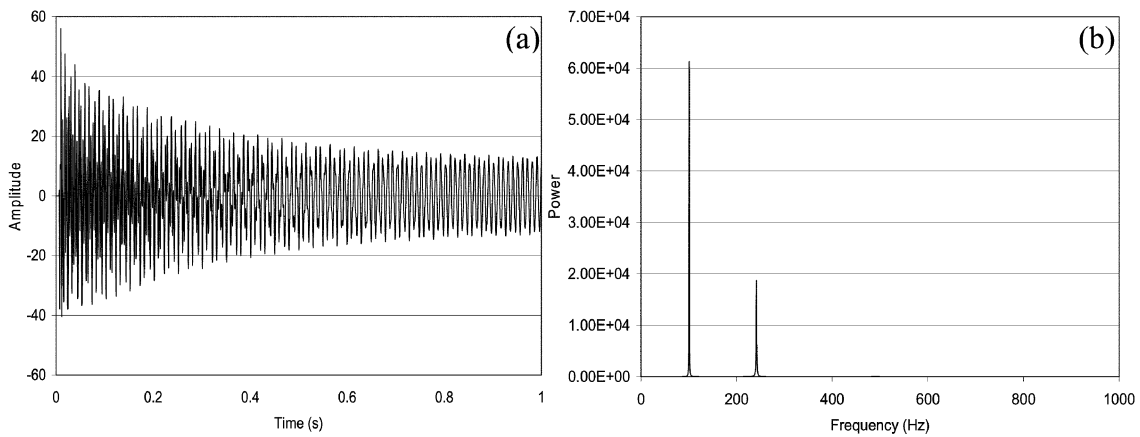


Fig. 4 (a) Dynamic response and corresponding (b) power spectrum for S3 in Fig. 1

frequency values (Quek, *et al.* 2003b), thus giving more precise peak energy values for computation of the FRF. Another reason is the simplicity in the application of the FFT.

An example of the power spectrum via FFT is shown in Fig. 4 for the dynamic response of point S3 in Fig. 1. By dividing the power spectrum of the response ( $R(\omega)$ ) by that of the impact load ( $F(\omega)$ ), the FRF ( $\alpha(\omega)$ ) is then obtained as given in Eq. (6) (Ewins 1984) (see Fig. 5).

$$\alpha(\omega) = \frac{R(\omega)}{F(\omega)} \quad (6)$$

Depending on the dynamic response measured ( $R(\omega)$ ), if the response collected is displacement, then the receptance FRF is obtained; if velocity or acceleration is measured, then mobility or inertance / accelerance FRF will be obtained respectively. The FRF values for different modes (see Fig. 5) can be obtained similarly for each of the measured points along the beam. Fig. 2(a) shows the plot of the normalized FRF values for each mode. Nonetheless, it is evident (see Fig. 2(a)) that these values do not give the analytical mode shape values. This is because the FRF are obtained from the power spectrum of the response and impact, and not the energy spectrum. By taking the square root of the FRF values, the normalized mode shapes obtained will then give similar results to the analytical mode shapes as

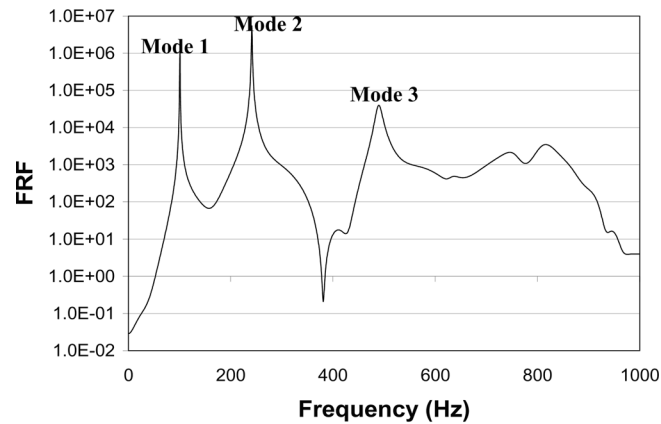


Fig. 5 Frequency response function for S3 in Fig. 1

shown in Fig. 2(b). Hence, from these results it is discernible that the FRF values from the energy spectrum for the different modes are analogous to the corresponding mode shape coefficients.

It must be stressed that the adoption of the FRF values for obtaining the modal parameter plays a key role in this method. This is largely because the FRF is able to produce a consistent result by normalizing the response by the excitation. As such, this aids in reducing the requirement of sensors at any one time, as data for different points may be collected separately but yet giving the same FRF values. The consistency of the FRF will be exhibited both numerically and experimentally in the following sections.

### 3. Finite element simulation

To illustrate the methodology described in the preceding section, the case of a damaged simply-supported aluminum plate is simulated numerically using ABAQUS 6.3 in this section. The plate measures  $500 \times 500 \times 2$  mm with properties given in Table 1.

Two cases of damage are considered, namely a single damage with varying degrees of severity and multiple damages with various combinations of severity of damage. To demonstrate the consistency of the FRF, the results of different load functions on the plate under the same state of health will also be studied.

#### 3.1. Single damage location

In this first case, damage is simulated by imposing a reduction in the Young's modulus,  $E$  for a small region in the plate. The position of the damage considered is a square area measuring  $15.625 \times 15.625$  mm with its lower left corner located at 156.25 mm both horizontally and vertically from a

Table 1 Properties of aluminum plate

Young's modulus, $E$ (GPa)	69.0
Shear modulus, $G$ (GPa)	26.5
Poisson's ratio, $\nu$	0.3
Mass density, $\rho$ (kg/m <sup>3</sup> )	2700

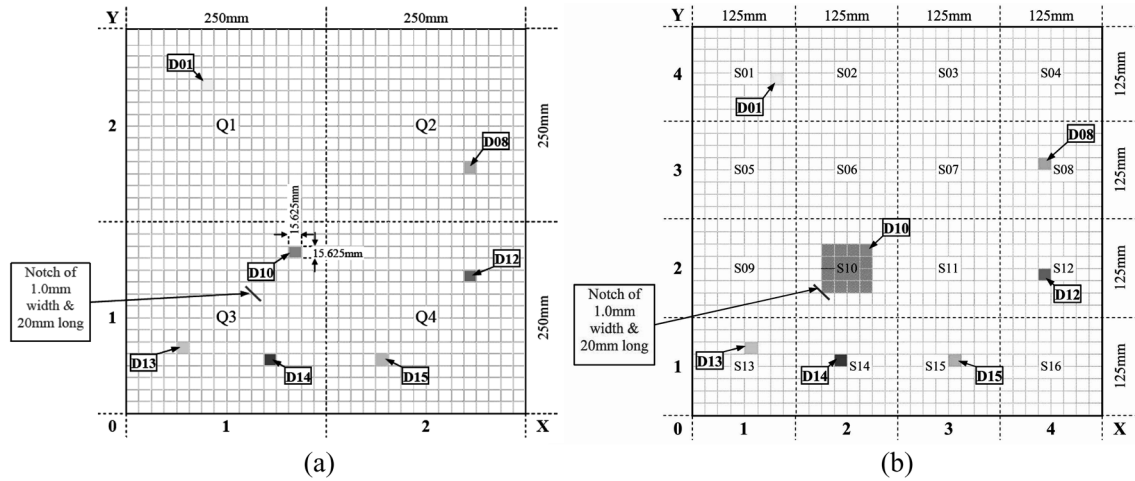


Fig. 6 Division of plate into (a) 4 (Q1-Q4) and (b) 16 (S01-S16) monitoring regions

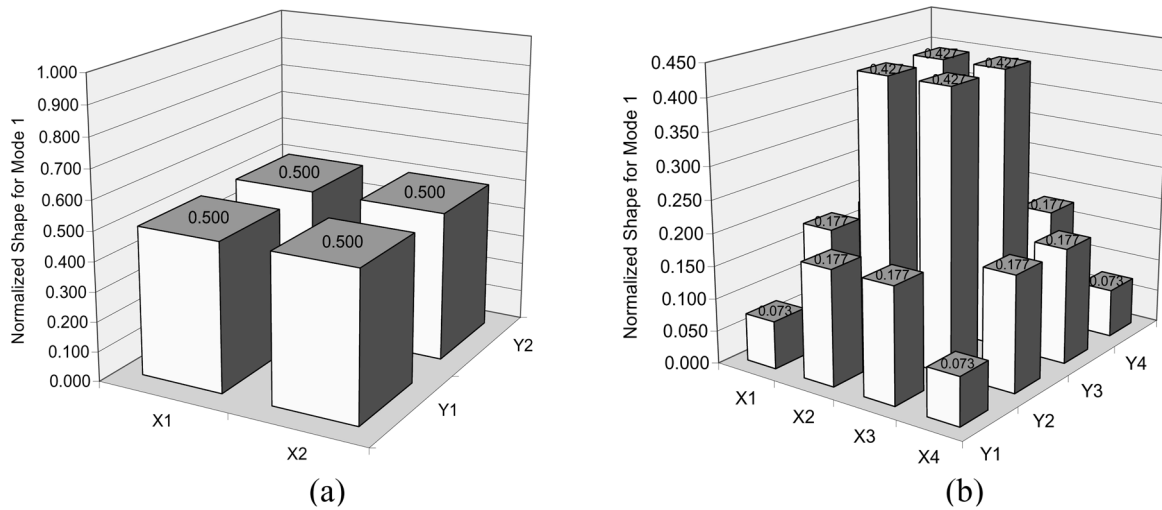


Fig. 7 Normalized shape for mode 1 of square plate using (a) 4 and (b) 16 points

corner of the plate (marked as D10 in Fig. 6). To illustrate the progressive zoning onto the damage location, the square plate is divided into 4 and 16 equal regions with the monitoring points at the centre of each region as shown in Fig. 6(a)-(b). The analytical normalized mode shape for the first mode (corresponding to modal frequency of 38.6 Hz) based on 4 and 16 points are given in Fig. 7(a) and (b) respectively.

For the damage location at D10 in Fig. 6, six degrees of damage severity, from 10% to 60% reduction in  $E$  in steps of 10%, are simulated. An impact load as illustrated by Fig. 3 (with peak amplitude of 5N) is imposed at the centre of the square plate and the dynamic responses at the monitoring points are collected and processed via FFT. In this study, the acceleration responses are collected and the accelerance FRF can be computed for each point. The FRF values corresponding to the first mode are obtained at the monitored points and the mode shape coefficients for the first mode can be computed as described in the preceding section.

686.62 (Q1)	686.62 (Q2)
686.62 (Q3)	686.62 (Q4)

201.14 (S01)	458.54 (S02)	458.54 (S03)	201.14 (S04)
458.54 (S05)	1172.20 (S06)	1172.20 (S07)	458.54 (S08)
458.54 (S09)	1172.20 (S10)	1172.20 (S11)	458.54 (S12)
201.14 (S13)	458.54 (S14)	458.54 (S15)	201.14 (S16)

(a) (All units in  $\text{ms}^{-2}/\text{N}$ ) (b)

Fig. 8 Simulated accelerance FRF values of undamaged plate for (a) 4 and (b) 16 points

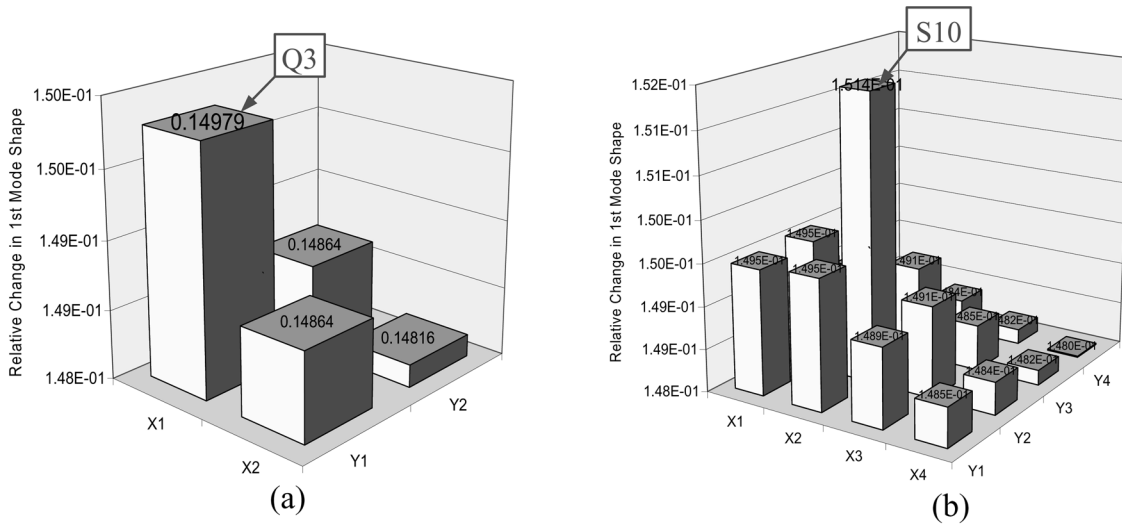


Fig. 9 Relative change in mode 1 for 50% reduction in  $E$  at D10 using (a) 4 and (b) 16 points

The accelerance FRF values of the healthy plate for 4 and 16 points are depicted in Fig. 8(a) and (b). The normalization of these values correspond exactly to the normalized mode shape coefficients obtained analytically (Fig. 7(a) and (b)) which is in agreement with the preceding section. Next, the FRF values for the simulated damaged conditions of the plate are estimated. It is observed that the frequency of the first mode remains unchanged (38.6 Hz) for all the six damage cases, which implies either virtually no damage or presence of a fine localized damage. The relative change in the first mode shape for the damage cases to the healthy case is then computed as outlined earlier in Section 2. Fig. 9 shows the results obtained for the 50% reduction in  $E$ , which corresponds well to the actual damage location. The highest positive relative change in values occurs in region Q3 and S10 for the 4 and 16 partitions respectively where D10 is located (see Fig. 6).

From the results obtained in Fig. 9, it is evident the 16 partition plate can be perceived as a refined zoning onto the damage location from initial 4 partitions. By further partitioning the region of S09, S10, S13 and S14 (Fig. 6) into 16 equal partitions with each of these consisting of 4 partitions (A-D) (see Fig. 10(a)), the damage D10 is now confined within region S10B. The result of the computed relative changes in the mode shape based on mode 1 is shown in Fig. 10(b) where the identified damage region

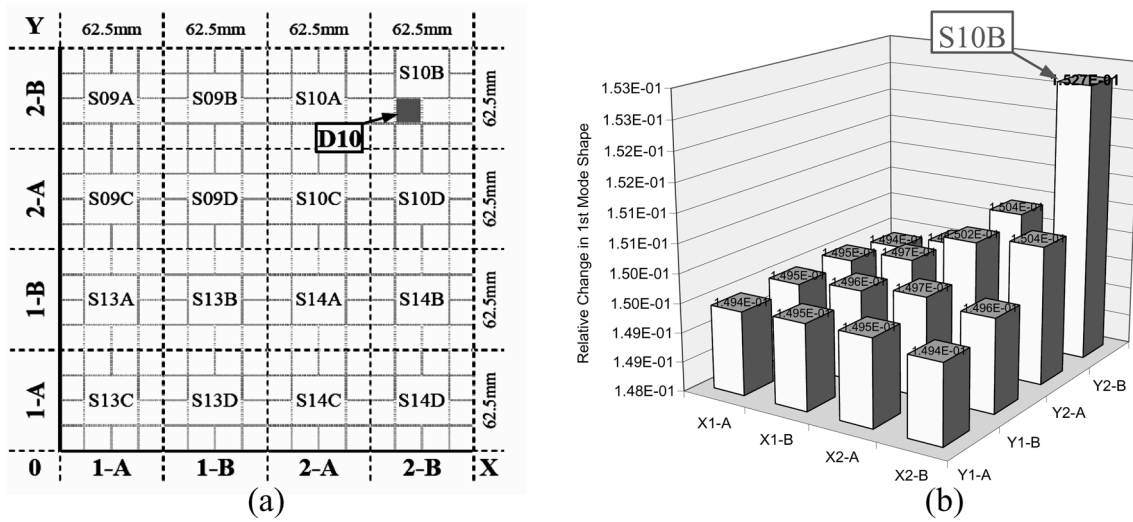


Fig. 10 (a) Further partitioning of region S09, S10, S13 and S14 in Fig. 6 into 16 regions, and (b) relative change in mode 1 for 50% reduction in  $E$  at D10

is S10B which corresponds to the actual location in Fig. 10(a).

A summary of the maximum relative change in first mode shape for the different degrees of damages based on the 4 and 16 partitioning of the entire plate (i.e. Q3 and S10 respectively) is given in Fig. 11. The maximum relative change in the mode shape values increases with the severity of damage, and hence, the relative change can be used as a gauge on the severity of the damage. Note that this example corresponds to cases where the change in modal frequency is small (i.e. cases with fine localized damage).

To further demonstrate the feasibility of the method for the single damage case for other areas of the plate, damages with 50% reduction in  $E$  at positions D13 and D14 indicated in Fig. 6 are studied. The results of the relative change in the first mode shape for these two damage locations are depicted in Figs. 12 and 13, which again exhibits the feasibility of the method in identifying monitored positions nearest to the damage. From these results, it can also be observed that the damages at different positions

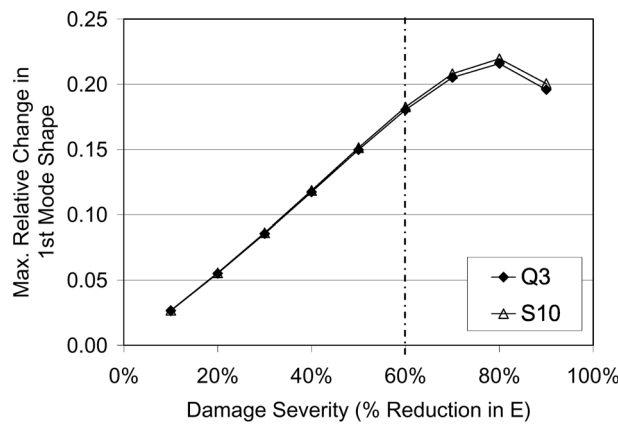


Fig. 11 Maximum relative change in mode 1 for varying severity of damage at D10

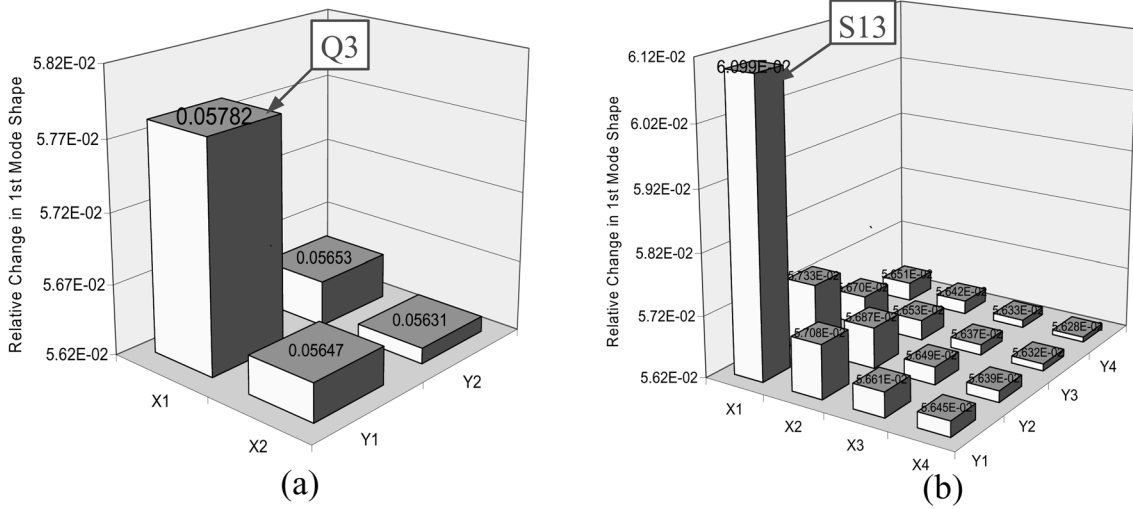


Fig. 12 Relative change in mode 1 for 50% reduction in  $E$  at D13 using (a) 4 and (b) 16 points

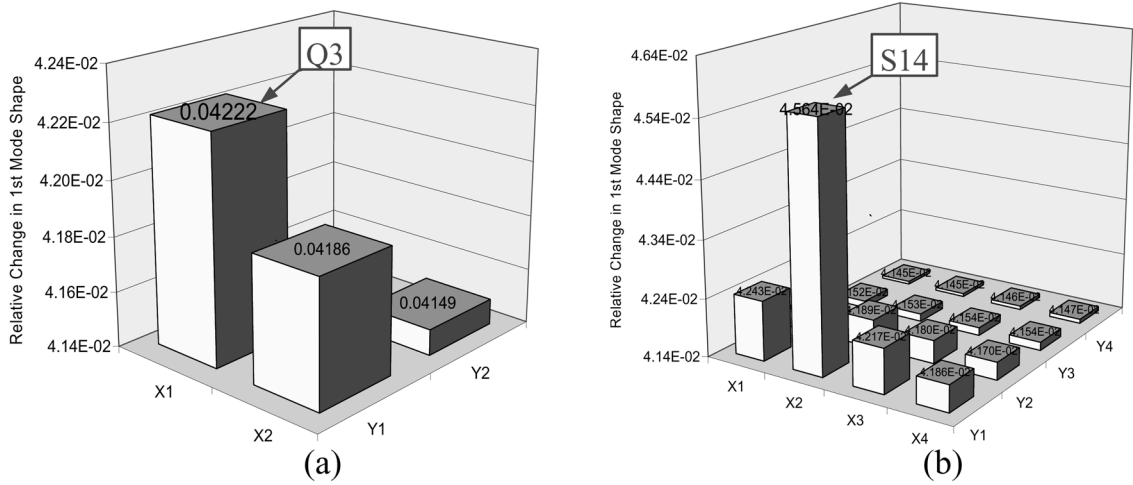


Fig. 13 Relative change in mode 1 for 50% reduction in  $E$  at D14 using (a) 4 and (b) 16 points

produce different amounts of relative change in the mode shape given the same severity in damage (50% reduction in  $E$ ). For example, considering the partitioning of the plate into 16 regions, for the same amount of damage (50% reduction in  $E$ ), the maximum relative change at D10 is  $1.514 \times 10^{-1}$ , at D13 is  $6.10 \times 10^{-2}$  and at D14 is  $4.564 \times 10^{-2}$ . In these cases, the relative change for D13 and D14 are both lower than D10 (one order lower) because their positions are nearer to the boundary and hence a damage of the same amount produce less effect at these positions resulting in the lower change.

In the above cases, all the damages are simulated by reducing  $E$  and a positive relative change in the mode shape is observed. It is of interest to investigate if the reverse (i.e. an increase in the  $E$ ) will produce a converse result. As such, a 20% increase in  $E$  is assumed for the region D10 in Fig. 6. The relative change in the first mode shape is computed similarly and the results are given in Fig. 14. Again, no detectable change in the modal frequency is observed. From Fig. 14, negative relative changes for all the monitored points are observed, with the highest absolute change occurring at Q3 and S10 for the

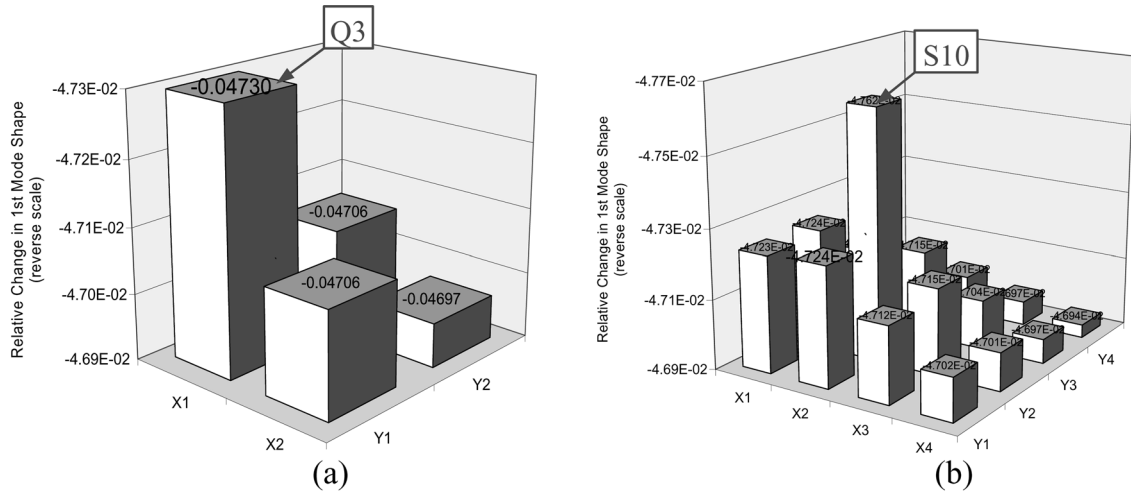


Fig. 14 Relative change in mode 1 for 20% increase in  $E$  at D10 using (a) 4 and (b) 16 points

4 and 16 monitored points respectively, and these corresponds to the points closest to D10. From this result, it may be deduced that the proposed method has the potential to differentiate whether a damage or a stiffening has occurred over a localized region.

### 3.2. Multiple damage locations

It will be of practical interest to examine if the same methodology can be extended to the case of multiple damages on the plate, including various combinations of damage severity. In this section, the plate with the same specifications, dimensions and boundary as the preceding section is considered.

The first case examined is that with a 50% reduction in  $E$  at both regions D08 and D10 (see Fig. 6). The relative changes in the mode shape values compared to the healthy case in the preceding section for

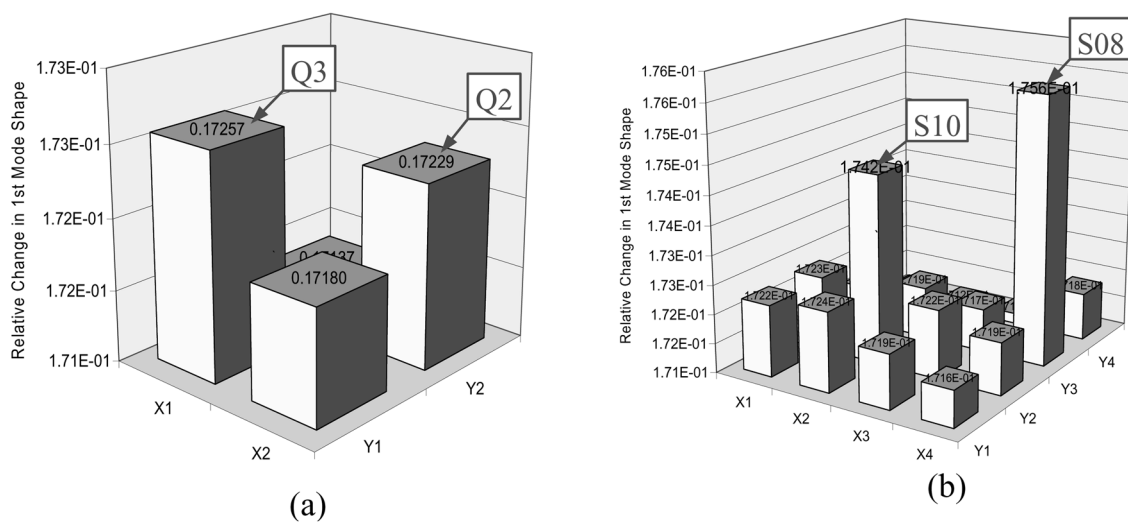


Fig. 15 Relative change in mode 1 for 50% reduction in  $E$  at D08 and D10 using (a) 4 and (b) 16 points

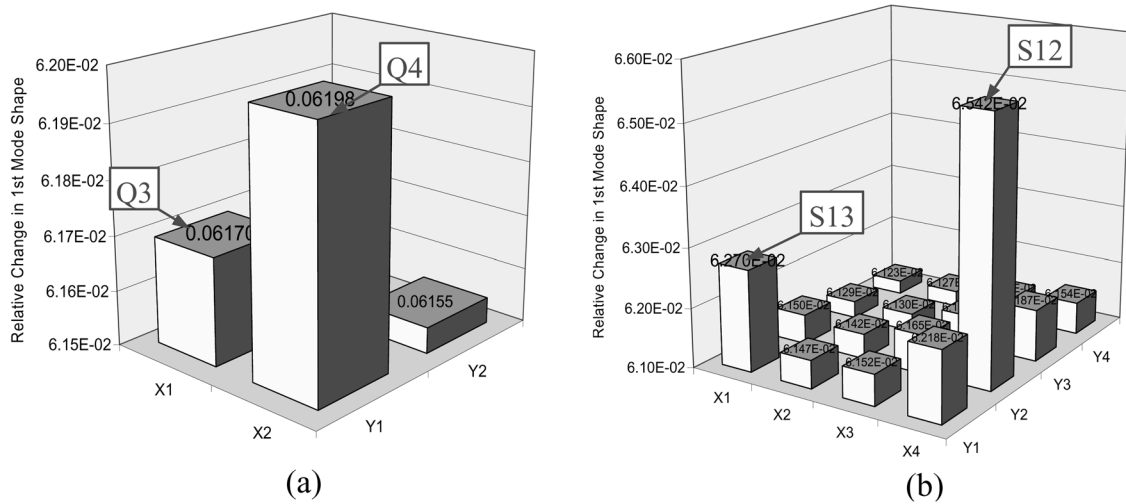


Fig. 16 Relative change in mode 1 for 50% and 20% reduction in  $E$  at D12 and D13 respectively using (a) 4 and (b) 16 points

mode 1 are given in Fig. 15. The results showed that the higher positive relative changes occur at quadrants Q2 and Q3 (Fig. 15(a)) which contain the damaged regions D08 and D10 respectively. Likewise, the two highest changes also occur in regions S08 and S10 for the 16 partition plate (Fig. 15(b)) which are the closest monitored positions to damages D08 and D10 respectively.

Two other combinations of dual-point damages with differing severity are studied. The purpose of studying these two damage configurations is to investigate if damage at one location may have an overwhelming effect at another due to their positions and differing severity, resulting in obscuring the relative change in mode shape for that damage region. The first consists of a 50% and 20% reduction in  $E$  for damage zones D12 and D13 respectively (see Fig. 6). The two damage positions are well separated on the plate. The results of the relative change in the first mode shape compared to the healthy case are given in Fig. 16. From these results it can be seen that the location of the damage is distinctly isolated to quadrants Q3 and Q4 and S12 and S13 for the 4 and 16 partitions respectively (Fig. 16(a) and (b)). It is also observed that the relative change for Q4 and S13 are higher than Q3 and S12 respectively, which correlates to the higher degree of damage for the case of position D12 over D13. In the second example, a 50% and 20% reduction in  $E$  at damage zones D10 and D13 respectively (see Fig. 6) is studied. Likewise, the relative change in the first mode shape with respect to the healthy case is computed and the results depicted in Fig. 17. The isolation of the damage is successful with the highest relative change observed at Q3 for the 4 quadrants and at S10 and S13 for the 16 partitions cases. However, the difference in the severity for the two damage positions (D10 and D13) is not significantly distinct for the case of 16 partitions (see Fig. 17(b)). This may be due to the proximity of the two monitored positions, which resulted in the higher relative change observed for the monitored position S13.

To illustrate the feasibility of the methodology with more damage zones, a four-damage zones case is studied. The four damage positions considered are D1, D8, D10 and D15 (Fig. 6), with a 50% reduction in  $E$  for each position. From the results of the relative change in mode shape values for the 4 quadrants depicted in Fig. 18(a), one may be inclined to conclude that the damage is isolated within Q3, although all four quadrants actually contain damages (see Fig. 6). This example indicates that the results obtain

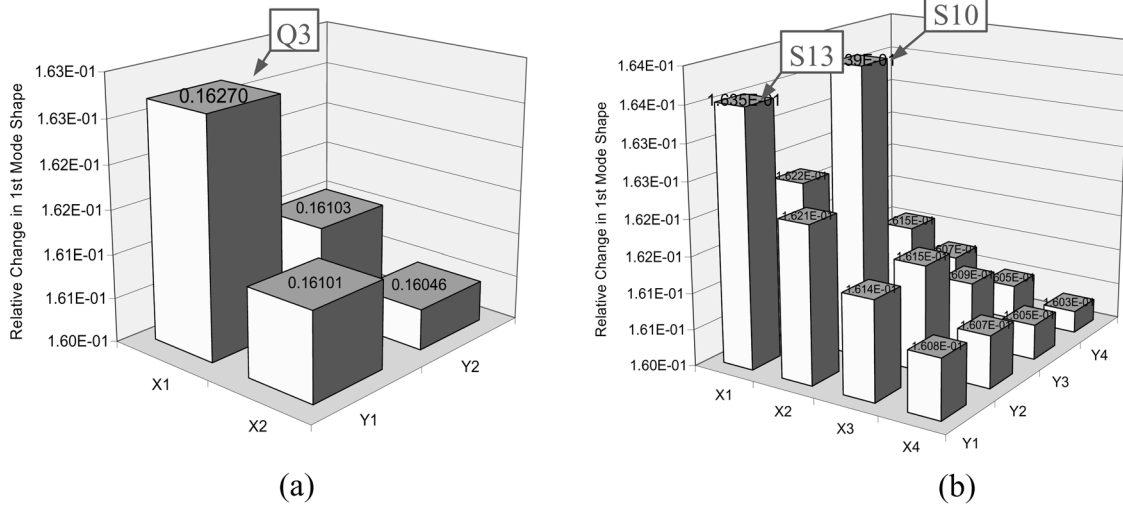


Fig. 17 Relative change in mode 1 for 50% and 20% reduction in  $E$  at D10 and D13 respectively using (a) 4 and (b) 16 points

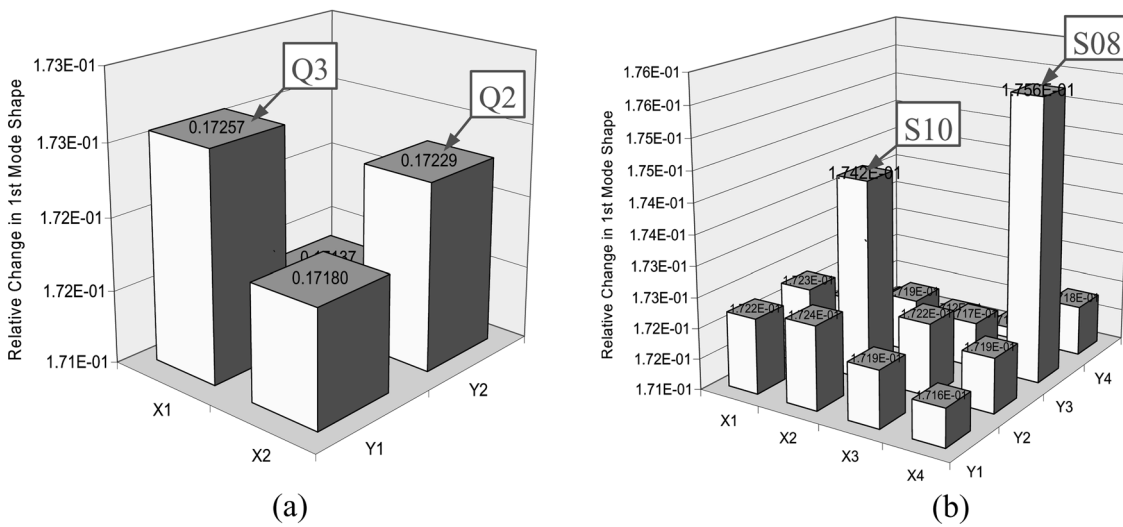


Fig. 18 Relative change in mode 1 for 50% reduction in  $E$  at D1, D8, D10 and D15 using (a) 4 and (b) 16 points

from the four monitored positions is inadequate to provide clear conclusion on the damage zones. On the other hand, if 16 partitions are used, the results (Fig. 18(b)) clearly show the changes in the four damage regions by sensors S1, S8, S10 and S15 relative to those in other regions. Thus, one may deduce that a 16 partition strategy is needed to confirm the results of a 4 partition monitoring system. Nevertheless, the simulation examples presented above demonstrate numerically the feasibility of the method.

### 3.3. Consistency of FRF under varying impacts

In the above numerical simulations, an identical impact load has been adopted for all cases. Nonetheless, it must be noted that in practical situation this may not be feasible. As such, the adoption of FRF is often seen as a means to achieve consistent results for the mode shape values at each state of the structure for varying load conditions. This important point has not been investigated in the preceding sections.

Generally, the impact loading may vary in two ways, namely, (a) the strength of impact and (b) the duration of contact which also determines the frequency band of the excitation load. The consistency of the FRF values obtained from differing impact loadings will be illustrated. To achieve this, the FRF results for the healthy state of the plate obtained using the impact load given in Fig. 3 from the previous simulation is used as a benchmark reference for comparison. This benchmark impact has contact duration of 0.015s and peak strength of 5N. FRF results for the same healthy plate obtained by three different impact loads via numerical simulation will be compared against this reference. The three different impacts considered are: (a) a similar impact as in Fig. 3 but with strength scaled up 10 times (i.e. peak at 50N), (b) an impact of same peak amplitude (5N) but having a longer contact time (0.040s) resulting in smaller excitation bandwidth (see Fig. 19) and (c) an impact similar to (b) but with strength scaled up by 5 times (i.e. peak at 25 N).

For case (a), the relative changes in the first mode accelerance FRF values for both the 4 and 16 monitored points are zero.

For case (b) (see Fig. 19), the differences in FRF values against the benchmark reference are given in Fig. 20. The differences observed due to this 0.025s difference in the contact duration of the impacts are fairly consistent at approximately  $-6.0 \times 10^{-5}$ , where the negative sign implies that the FRF values obtained by the impact in Fig. 19(a) is lower. The possible reason for this difference may be explained by the Fourier spectrum of the impacts and responses. As mention in Section 2, the FRF is obtained as the ratio of the response spectrum to that of the load spectrum (see Eq. (7)). For the impact described in Fig. 3(a), we observed broader spread in energy into the higher frequencies for its power spectrum (see Fig. 3(b)), i.e. a wider excitation band. On contrary, for the impact given in Fig. 19(a) the energy is more concentrated at relatively lower frequency band (see Fig. 19(b)) and is of almost two orders higher than that for the benchmark impact (Fig. 3(b)). Next, we observe the response for a monitored point, say Q1 (see Fig. 6) due to these two impacts (Fig. 3 and 19) on the healthy plate, whereby the

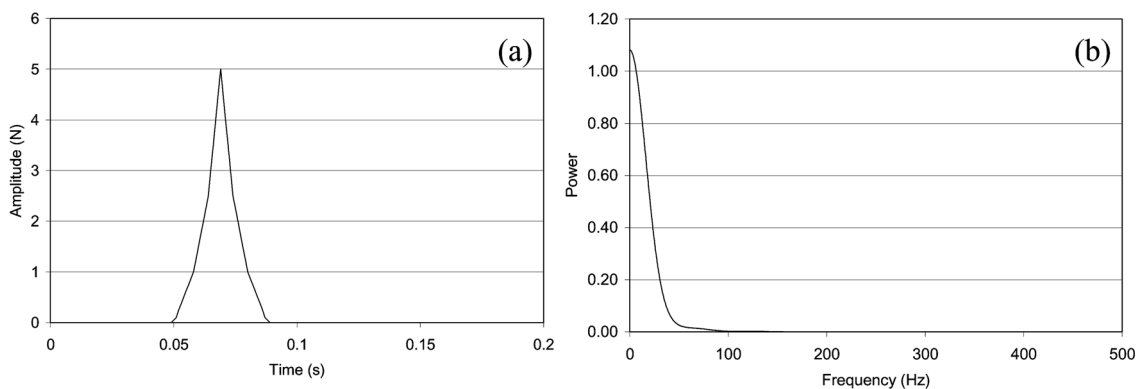


Fig. 19 (a) Impact load with longer contact and corresponding (b) power spectrum

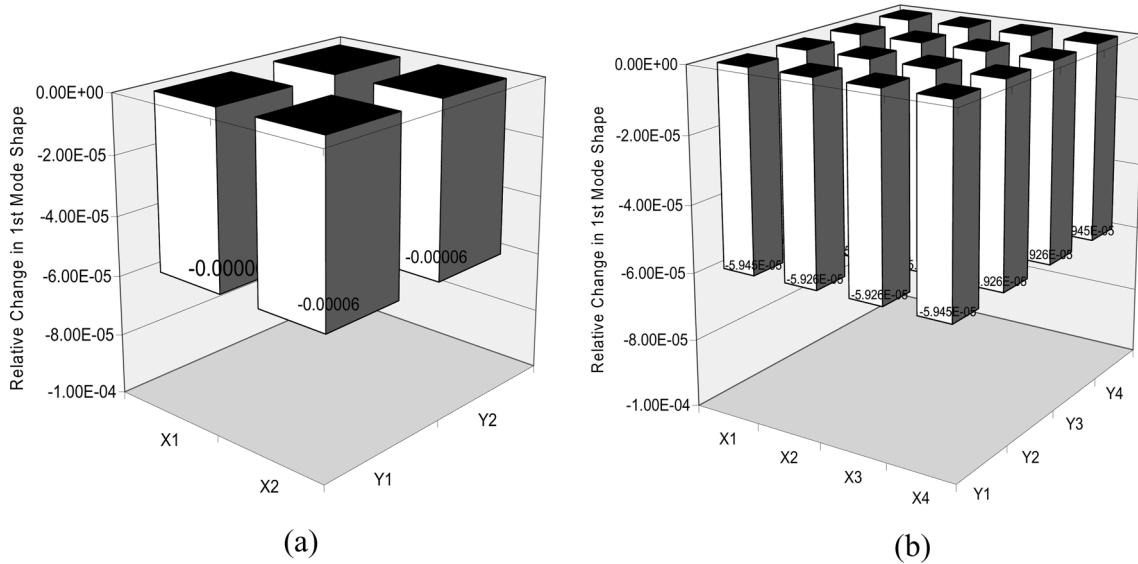


Fig. 20 Relative change in mode 1 for using impact load with longer contact time for (a) 4 and (b) 16 points

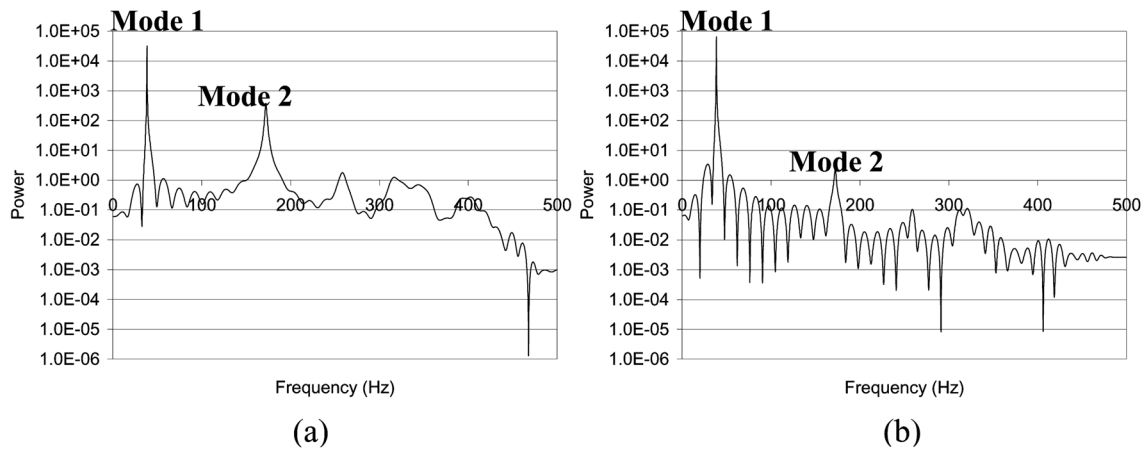


Fig. 21 Power spectrum of response at monitored point Q1 in Fig. 6 under impact load described by (a) Fig. 3 and (b) Fig. 19

Fourier spectra are as depicted in Fig. 21. From Fig. 21, it can be observed that both impacts produced a mode 1 response of the same order of magnitude ( $3.19 \times 10^4$  and  $6.45 \times 10^4$  by impacts in Fig. 3 and 19 respectively). Hence, when taking the ratio of the spectrum between the response and the impact for the FRF values, the impact in Fig. 19(a) thus produces lower FRF values due to the higher radical base albeit the peak magnitude for both impacts are the same (5N). Nonetheless, the difference in the accelerance FRF values of  $-6.0 \times 10^{-5}$  is still three orders of magnitude lower than the maximum difference observed for the single damage D10 simulated by a 10% reduction in  $E$  ( $2.68 \times 10^{-2}$ ).

For case (c), the results in Fig. 20 are also obtained, which show that the FRF values obtained by the third impact are similar to that by the second impact.

It can be deduced that variation in the strength of the same impact does not influence the FRF

consistency as depicted in the results of the first impact with the benchmark and the third impact with the second. However, the variation in the contact time of the impact does produce some variations, such as that observed between second impact and the benchmark. Large variation in the impact loading especially in terms of the contact duration may therefore produce differences in results for the structure under the same health state. This means the threshold for the smallest detectable damage has to be raised reducing the attractiveness of the method. This observation is consistent with that pointed out by Hwang (1998) and Hwang and Kim (2004) where practical computation of FRF values suffers from inaccuracies caused by experimental errors.

### 3.4. Limitations of proposed method

It is observed so far that reduction in  $E$  consistently produced an increase in the mode shape values. This may be explained using Eq. (2). By taking its derivative with respect to time, the acceleration of the free vibration response may be obtained as  $-U\omega^2 e^{i(\omega t + \theta)}$ . With a decrease in the stiffness of the structure, the amplitude of vibration ( $U$ ) is generally increased. However, since the damage is localized and small, the change in the structural frequency ( $\omega$ ) is almost negligible, and the value of the term  $\omega^2 e^{i(\omega t + \theta)}$  is virtually unchanged. The overall increase in the vibration energy as a result of the increase in amplitude causes a positive relative change in the mode shape values based on the computation described in Eq. (5).

In cases where the damages are more severe or cover a substantial zone, changes in the modal frequencies may be significant. The feasibility of the proposed methodology needs to be investigated.

For this purpose, a further reduction in the  $E$  (70%, 80% and 90%) for damage location D10 described in Fig. 6 is studied. It is observed that the first modal frequency for 70% reduction in  $E$  remains unchanged at 38.6 Hz whereas it decreases to a value of 38.2Hz for the cases of 80% and 90% reduction in  $E$ . The maximum relative change in first mode FRF values for these degrees of damages based on the 4 and 16 partitions of the entire plate (i.e. Q3 and S10 respectively) are also summarized in Fig. 11. For the case of 70% reduction in  $E$ , a higher relative change is observed compared to that of 60%, as expected. What is not obvious is the change in trend beyond 80% reduction in  $E$ . This also corresponds to the point where a drop in the modal frequency is observed.

Next, the case of a larger damage zone is examined by extending D10 by 16 times to the area shaded by diagonal lines in Fig. 6(b). This damage is still within the quadrant Q3 and region S10. A reduction of 50% in  $E$  is simulated and the acceleration FRF values for the first mode is obtained for the 4 and 16 sensor points and compared with those from the healthy plate. A decrease in the first modal frequency to a value of 38.0Hz is observed. The results of the relative change of the FRF values corresponding to the first mode are as shown in Fig. 22. It can be noted that the maximum relative change again occurs at Q3 and S10, with values of  $8.938 \times 10^{-2}$  and  $1.056 \times 10^{-1}$  respectively, indicating the proximity of these monitored points to the damage. Since this current damage is one of a larger extent (i.e. more severe), it is expected that the relative changes is larger than the previous smaller D10 damage for the same 50% reduction in  $E$ . On the contrary, the values obtained  $1.498 \times 10^{-1}$  for Q3 and  $1.514 \times 10^{-1}$  for S10 are lower (see Fig. 9).

The two above cases of damages, one with higher severity and the other with a larger extent, exhibit decrease in modal frequency and an unexpected lower relative change in the FRF values. The reason for the latter becomes obvious when one examines the acceleration term,  $-U\omega^2 e^{i(\omega t + \theta)}$ . Although  $U$  may increase due to damage, the drop in  $\omega$  has a squared contribution. This results in a significant decrease in the overall acceleration unlike that when displacement FRF values are considered. This causes the

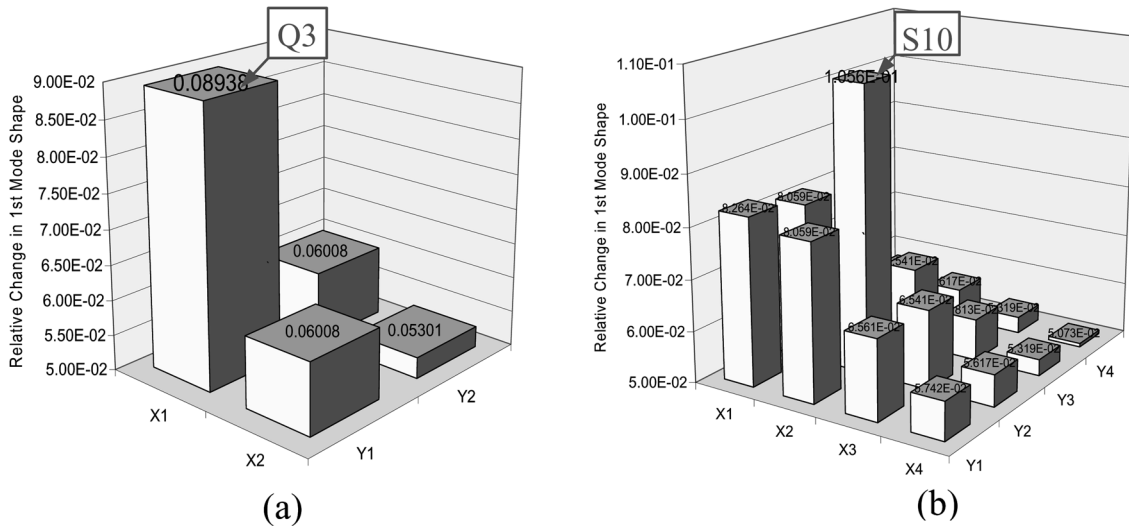


Fig. 22 Relative change in mode 1 for 50% reduction in E at extended D10 region using (a) 4 and (b) 16 points

apparent breakdown in the positive trend between acceleration FRF-based mode shape coefficients and the severity of damage presented in Section 2.

However there is no cause for despair if one checks the change in modal frequency values first. A detectable decrease (outside the range of experimental error) in modal frequency does often imply an anomaly analogous to the presence of damage. The damage in such case can be confirmed by the use of displacement rather than acceleration FRF values may be more meaningful although the former is harder to monitor in practice currently. On the other hand, if there is no detectable change in the modal frequency, then the proposed methodology may be used to test the presence of fine cracks or localized damage zones.

#### 4. Experimental verification

To verify the applicability of the proposed method for practical problems, a square aluminum plate of same geometry ( $500 \times 500 \times 2$  mm) and material properties (see Table 1) as that of the numerical example presented earlier is used. PCB Piezotronics, Inc. impact hammer (Model: 086B03) and accelerometers (Model: 353B14) are used to provide the impact loading and monitoring of accelerations at specific positions respectively.

In this experiment, the undamaged state of the plate is first assessed. Similar to the numerical example, the plate is partitioned into 4 and 16 regions (Fig. 6) for the initial and refined detection of damage zones respectively. The accelerations of the 4 and 16 monitored points under free vibration are collected by manually inducing a short duration impact load at the centre of the plate using the impact hammer. Following the procedure presented in the earlier section, the acceleration FRF is first obtained and the results corresponding to the first fundamental mode shown in Fig. 23. The FRF values obtained from each point is an average from 50 impacts, to minimize the inconsistency in FRF caused by the difference in contact time of the impacts as illustrated in the preceding discussion. Table 2 gives a summary of the average FRF values for each point with the corresponding standard deviations for the

60.056 (Q1)	60.448 (Q2)	19.476 (S01)	43.040 (S02)	43.441 (S03)	19.087 (S04)
60.167 (Q3)	62.627 (Q4)	46.445 (S05)	106.035 (S06)	107.015 (S07)	46.734 (S08)
		44.334 (S09)	107.552 (S10)	106.216 (S11)	44.902 (S12)
		18.376 (S13)	44.333 (S14)	46.289 (S15)	19.855 (S16)

(a) (All units in  $\text{ms}^{-2}/\text{N}$ ) (b)

Fig. 23 Accelerance FRF values of undamaged plate for (a) 4 and (b) 16 points

Table 2 Summary of experimental FRF values corresponding to first mode for undamaged plate

Sensor Position	No. of Samples	Mode 1 Freq (Hz)	FRF ( $\text{ms}^{-2}/\text{N}$ )	Standard Deviation
Q1	50	39.4	60.056	2.304 3.84%
Q2	50	39.4	60.448	2.241 3.71%
Q3	50	39.4	60.167	2.394 3.98%
Q4	50	39.4	62.627	1.414 2.26%
S01	50	39.4	19.476	1.583 8.13%
S02	50	39.4	43.040	1.115 2.59%
S03	50	39.4	43.441	1.920 4.42%
S04	50	39.4	19.087	0.824 4.32%
S05	50	39.4	46.445	0.925 1.99%
S06	50	39.4	106.035	5.009 4.72%
S07	50	39.4	107.015	4.495 4.20%
S08	50	39.4	46.734	1.383 2.96%
S09	50	39.4	44.334	2.446 5.52%
S10	50	39.4	107.522	4.287 3.99%
S11	50	39.4	106.216	4.422 4.16%
S12	50	39.4	44.902	2.609 5.81%
S13	50	39.4	18.376	0.675 3.68%
S14	50	39.4	44.333	2.112 4.76%
S15	50	39.4	46.289	2.280 4.93%
S16	50	39.4	19.855	0.721 3.63%

Note: see Fig. 6 for sensor positions

healthy plate.

To compare the experimental and numerical results, first it is noted that the points may be grouped based on the symmetry of the plate and the mean values of each group used. Both sets of values can then be normalized by their respective highest group value (Group: S6 / S7 / S10 / S11) and the results are tabulated in Table 3. It can be seen that the experimental results for the undamaged plate is very similar to the simulation results. In addition, the frequency for the first mode obtained experimentally (39.4 Hz) is also close to that from simulation (38.6 Hz).

Table 3 Comparison of FRF values obtained for simulation and experiment

Group (Sensor Position)	Ave Expt. FRF (Group) ( $\text{ms}^{-2}/\text{N}$ )	Simul. FRF ( $\text{ms}^{-2}/\text{N}$ )	*Ratio	
			Expt.	Simul.
Q1 / Q2 / Q3 / Q4	60.824	686.62	0.570	0.585
S6 / S7 / S10 / S11	106.697	1172.20	1.000	1.000
S1 / S4 / S13 / S16	19.198	201.14	0.180	0.172
S2 / S3 / S5 / S8 / S9 / S12 / S14 / S15	44.940	485.54	0.421	0.414

\*Taken as the ratio of the FRF values to the highest FRF value for both the experiment & simulation.

Note: see Fig. 6 for sensor positions.

Table 4 Summary of experimental FRF values corresponding to first mode for plate with half-through notch

Sensor Position	No. of Samples	Mode 1 Freq (Hz)	FRF ( $\text{ms}^{-2}/\text{N}$ )	Standard Deviation	
Q1	50	39.4	69.081	3.228	4.67%
Q2	50	39.4	68.468	3.118	4.56%
Q3	50	39.4	70.252	3.329	4.74%
Q4	50	39.4	71.751	3.075	4.29%
S01	50	39.4	22.267	1.287	5.78%
S02	50	39.4	48.989	2.550	5.20%
S03	50	39.4	48.897	2.130	4.36%
S04	50	39.4	21.597	1.085	5.02%
S05	50	39.4	53.171	2.661	5.01%
S06	50	39.2	121.659	3.996	3.28%
S07	50	39.2	121.444	3.653	3.01%
S08	50	39.4	52.678	2.696	5.12%
S09	50	39.4	51.435	1.862	3.62%
S10	50	39.2	127.215	4.277	3.36%
S11	50	39.2	122.554	3.966	3.24%
S12	50	39.4	51.192	2.831	5.53%
S13	50	39.4	21.368	0.947	4.43%
S14	50	39.4	51.398	2.772	5.39%
S15	50	39.4	52.981	2.562	4.84%
S16	50	39.4	22.518	1.705	7.57%

Note: see Fig. 6 for sensor positions

Based on the procedures described in Section 2, the relative change in the FRF values corresponding to first mode of the plate, which are also representative of the first mode shape coefficients, obtained are shown in Fig. 24. Fig. 24(a) shows that Q3 experiences the highest relative change, and Fig. 24(b) clearly gives S10 with the highest change. Both these results correspond to the location of the monitored points closest to the induced damage (see Fig. 6).

Subsequently, the notch on the plate is deepened through the thickness of the plate and the acceleration response of the sensor points from 50 manual impacts at the centre of the plate recorded. The acceleration FRF values are computed for the 4 and 16 monitored points and the results summarized in Table 5. The modal frequencies for all the monitored points decreased to 39.2 Hz or

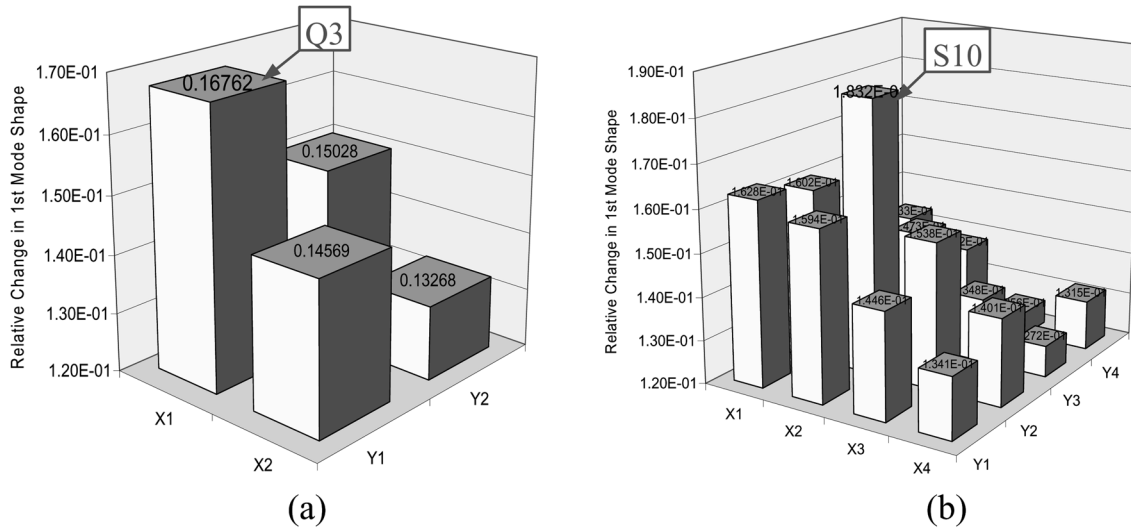


Fig. 24 Relative change in mode 1 for plate with half-through notch using (a) 4 and (b) 16 points

Table 5 Summary of experimental FRF values corresponding to first mode for plate with through notch

Sensor Position	No. of Samples	Mode 1 Freq (Hz)	FRF ( $\text{ms}^{-2}/\text{N}$ )	Standard Deviation
Q1	50	39.2	66.377	2.295 3.46%
Q2	50	39.2	65.839	3.360 5.10%
Q3	50	39.2	67.475	3.331 4.94%
Q4	50	39.2	68.688	3.372 4.91%
S01	50	39.2	21.364	1.533 7.18%
S02	50	39.2	47.280	2.024 4.28%
S03	50	39.2	46.953	1.944 4.14%
S04	50	39.2	20.638	1.136 5.50%
S05	50	39.2	51.093	2.200 4.31%
S06	50	39.0	118.103	3.998 3.39%
S07	50	39.2	117.791	3.844 3.26%
S08	50	39.2	50.817	2.877 5.66%
S09	50	39.0	49.366	1.819 3.69%
S10	50	39.0	123.204	4.595 3.73%
S11	50	39.2	117.752	3.943 3.35%
S12	50	39.2	49.231	2.496 5.07%
S13	50	39.2	20.853	1.188 5.70%
S14	50	39.0	49.759	2.141 4.30%
S15	50	39.2	51.269	2.710 5.29%
S16	50	39.2	21.709	1.227 5.65%

Note: see Fig. 6 for sensor positions

lower, with the worst occurring at positions S6, S9, S10 and S14 to about 39.0 Hz (see Table 5). The likely reason for the higher decrease in the modal frequency for monitored positions S6, S9, S10 and S14 may be due to their proximity to the notch location.

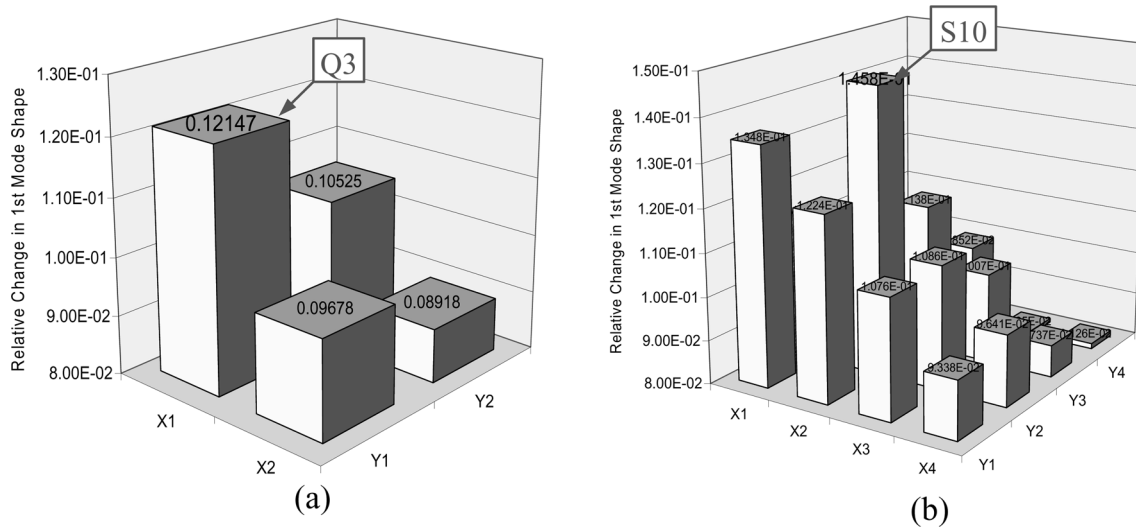


Fig. 25 Relative change in mode 1 for plate with through notch using (a) 4 and (b) 16 points

The relative changes of the FRF values corresponding to the first mode for the 4 and 16 monitored positions are computed as shown in Fig. 25. The highest relative changes are noted at Q3 and S10 for the 4 and 16 partitions (Fig. 25(a) and (b)) respectively. This can again be attributed to their proximity to the through notch. Compared to the previous case of the half-through notch (Fig. 24), a generally lower relative change is exhibited for this 'higher damage severity' (through notch) (Fig. 25). The reason for this is discussed in Section 3, where in cases of higher damage severities (such that the modal frequencies are altered), the relative change in the FRF values contributed by the increase in vibration amplitude is diminished by the decrease in the frequency.

The uncertainty arising from the variability in loading can be illustrated by examining the FRF results obtained for the three conditions of the plate, namely, undamage, half-through notch and through notch. The FRF values for all the monitored points experience some uncertainty, with different standard deviations computed from the 50 samples for each point (Tables 2, 4 and 5). This is due to the inconsistency in manual application of the impact load, which has been explained in Section 2. From Tables 2, 4 and 5, it can be observed that the uncertainties (standard deviation) for each of the points are generally kept below 6% with a couple near 8%. Therefore, for the impact used in this study, it is proposed that any relative change in the FRF values below 6% is insufficient to establish conclusively the presence of damage. For the two damage cases (half-through and through notches), both the highest relative changes in the FRF values are above 6% ( $1.832 \times 10^{-1}$  &  $1.458 \times 10^{-1}$ ).

## 5. Concluding remarks

To complement the methodology of scanning of the structure using Lamb wave propagation for the detection of fine damages such as cracks (as presented by Quek, *et al.* 2003a, 2004, Tua, *et al.* 2004a, b), a frequency domain method which utilizes the evaluation of changes in the structural mode shape is adopted for estimating the damage region. It is shown herein that the FRF values corresponding to the modal frequency is analogous to the mode shape coefficients for that particular mode. As such, the

monitoring of the maximum relative change in the FRF values with respect to the previously known state for different positions on the structure is adopted to detect possible damage zones. In this study, only the relative change in the FRF values for the first mode is considered because it is the most fundamental mode that can be easily excited for most structural form, and also every point in the structure will produce non-zero response in this mode as the nodal points are at the supports. The main advantage of the method is its simplicity in practical applications requiring only conventional signal processing technique (FFT). To overcome the variability in the impact loading at different instances and to cater for the possibility of insufficient sensors (requiring multiple impacts and shifting of sensors), the FRF is adopted to minimize inconsistency in the results. To further improve this, statistical averaging is recommended in practice. Despite these, large variations in the impact loadings should still be avoided where possible.

Numerical examples of an aluminum plate, which include damages of varying severity, locations and combinations of multiple locations, are presented to demonstrate the feasibility of the proposed method. An experimental verification of the method is also performed using an aluminum plate with two different degrees of damage, namely a half-through notch and a through notch. The method has shown to be viable for fine, localized damages whereby the change in the structural frequency is minimal as illustrated by both the numerical and experimental examples. Nonetheless, this method needs special attention when the damages induce notable changes in the modal frequency, such as when the damages are of high severity or cover more extensive area or near the boundary where support condition is modified. This is largely due to the significant decrease in the frequency term compared to the increase in the vibration amplitude. In the case of fine and/or highly localized cracks, this is not a concern. While this method is efficient in terms of identifying damage zones, it is nonetheless difficult to accurately locate the damage nor can it trace its actual geometrical extent. Hence, the wave propagation method presented in the earlier literature (Quek, *et al.* 2003a, 2004, Tua, *et al.* 2004a, b) can be employed efficiently for this purpose once the damage zone is identified.

## References

- Cawley, P. and Adams, R. D. (1979a), "The location of defects in structures from measurements of natural frequencies", *J. Strain Analysis*, **14**(2), 49-57.
- Ewins, D. J. (1984), *Modal Testing: Theory and Practice* (Research Studies Press, England).
- Hwang, H. Y. and Kim, C. (2004), "Damage detection in structures using few frequency response measurements", *J. Sound Vib.*, **270**(1), 1-14.
- Hwang, H. Y. (1998), "Identification techniques of structure connection parameters using frequency response functions", *J. Sound Vib.*, **212**(3), 469-479.
- Kim, J. T., Ryu, Y. S., Cho, H. M. and Stubbs, N. (2003), "Damage identification in beam-type structures: frequency-based method vs mode-shape-based method", *Eng. Struct.*, **25**, 57-67.
- Owolabi, G. M., Swamidas, A. S. J. and Seshadri, R. (2003), "Crack detection in beams using changes in frequencies and amplitudes of frequency response functions", *J. Sound Vib.*, **265**(1), 1-22.
- Pandey, A. K. and Biswas, M. (1994), "Damage detection in structures using changes in flexibility", *J. Sound Vib.*, **169**(1), 3-17.
- Quek, S. T., Jin, J. and Tua, P. S. (2004), "Comparison of plain piezoceramics and inter-digital transducer for crack detection in plates", *Smart Structures and Materials / NDE for Health Monitoring and Diagnostics 14-18 March, 2004, Town and Country Resort & Convention Center, San Diego, California USA*.
- Quek, S. T., Tua, P. S. and Wang, Q. (2003a), "Detecting anomaly in beams and plate based on Hilbert-Huang transform of real signals", *Smart Mater. Struct.*, **12**(3), 447-460.

- Quek, S. T., Tua, P. S. and Wang, Q. (2003b), "Comparison of hilbert-huang, wavelet and fourier transforms for selected applications", *Mini-Symposium on Hilbert-Huang Transform in Engineering Applications October 31 – November 01, 2003, Newark, Delaware*.
- Salawu, O. S. (1997), "Detection of structural damage through changes in frequency: A review", *Eng. Struct.*, **19**(9), 718-723.
- Samman, M. M. and Biswas, M. (1994a), "Vibration testing for nondestructive evaluation of bridges I: theory", *J. Struct. Eng.*, ASCE, **120**, 269-289.
- Samman, M. M. and Biswas, M. (1994b), "Vibration testing for nondestructive evaluation of bridges II: results", *J. Struct. Eng.*, ASCE, **120**, 290-306.
- Sampaio, R. P. C., Maia, N. M. M. and Silva, J. M. M. (1999), "Damage detection using frequency-response-function curvature method", *J. Sound Vib.*, **226**(5), 1029-1042.
- Schwarz, B. J. and Richardson, M. H. (1999), "Experimental modal analysis", *CSI 9th Annual Technology and Training Conference, Reliability Week, Oct 4-7 1999, Orlando, Florida USA*.
- Thyagarajan, S. K., Schulz, M. J. and Pai, P. F. (1998), "Detecting structural damage using frequency response functions", *J. Sound Vib.*, **210**(1), 162-170.
- Tua, P. S., Quek, S. T. and Wang, Q. (2004a), "Detection of cracks in plates using piezo-actuated Lamb waves", *Smart Mater. Struct.*, **13**(4), 643-660.
- Tua, P. S., Quek, S. T. and Wang, Q. (2004b), "Detection of crack in cylindrical pipes and plates using piezo-actuated Lamb waves", *Smart Mater. Struct.* (Under review).